Hindawi Publishing Corporation
Journal of Nanomaterials
Volume 2015, Article ID 620672, 11 pages
http://dx.doi.org/10.1155/2015/620672

Research Article

Ultra-Small Fatty Acid-Stabilized Magnetite Nanocolloids Synthesized by *In Situ* Hydrolytic Precipitation

Kheireddine El-Boubbou,[1,2] Rabih O. Al-Kaysi,[1,2] Muhanna K. Al-Muhanna,[3] Hassan M. Bahhari,[2] Abdulaziz I. Al-Romaeh,[3] Nadim Darwish,[4] Khaled O. Al-Saad,[2] and Salem D. Al-Suwaidan[2]

[1]*King Saud bin Abdulaziz University for Health Sciences (KSAU-HS), King Abdulaziz Medical City, National Guard Health Affairs, Riyadh 11481, Saudi Arabia*
[2]*King Abdullah International Medical Research Center (KAIMRC), King Abdulaziz Medical City, National Guard Hospital, Riyadh 11426, Saudi Arabia*
[3]*King Abdulaziz City for Science and Technology (KACST), Riyadh 11442, Saudi Arabia*
[4]*Departament de Química Física & Institut de Bioenginyeria de Catalunya (IBEC), Universitat de Barcelona, 08028 Barcelona, Spain*

Correspondence should be addressed to Kheireddine El-Boubbou; elboubboukh@ngha.med.sa

Received 6 March 2015; Revised 31 July 2015; Accepted 3 August 2015

Academic Editor: Mohmmad A. Malik

Simple, fast, large-scale, and cost-effective preparation of uniform controlled magnetic nanoparticles remains a major hurdle on the way towards magnetically targeted applications at realistic technical conditions. Herein, we present a unique one-pot approach that relies on simple basic hydrolytic *in situ* coprecipitation of inexpensive metal salts (Fe^{2+} and Fe^{3+}) compartmentalized by stabilizing fatty acids and aided by the presence of alkylamines. The synthesis was performed at relatively low temperatures (~80°C) without the use of high-boiling point solvents and elevated temperatures. This method allowed for the production of ultra-small, colloidal, and hydrophobically stabilized magnetite metal oxide nanoparticles readily dispersed in organic solvents. The results reveal that the obtained magnetite nanoparticles exhibit narrow size distributions, good monodispersities, high saturation magnetizations, and excellent colloidal stabilities. When the [fatty acid] : [Fe] ratio was varied, control over nanoparticle diameters within the range of 2–10 nm was achieved. The amount of fatty acid and alkylamine used during the reaction proved critical in governing morphology, dispersity, uniformity, and colloidal stability. Upon exchange with water-soluble polymers, the ultra-small sized particles become biologically relevant, with great promise for theranostic applications as imaging and magnetically targeted delivery vehicles.

1. Introduction

Lately, the continuous trials to produce controlled monodisperse magnetic metal oxide nanoparticles (M^3NPs) for both *in vitro* and *in vivo* endpoints have sky-rocketed [1]. In particular, the use of iron oxide (Fe_2O_3/Fe_3O_4) NPs in a variety of physioelectronic and biomedical applications offered M^3NPs a remarkable glow [2]. In fact, it has been shown that M^3NPs based on ferrites were applied to record storage devices, energy storage, catalysis, labeling cells, magnetically targeted imaging, drug delivery, and medical theranostics [1–3]. Various synthetic methods have been reported to produce M^3NPs, which include nonaqueous and aqueous sol-gel, microemulsion, sonochemical, and the most popular hydrothermal/solvothermal techniques [3]. Of the many available approaches, two main synthetic solution-based routes [4] have been popularized: (a) basic aqueous *coprecipitation* [5] of iron salts (as demonstrated by Massart) in the presence or absence of surfactants/polymers [6], (b) *high-temperature thermal decomposition* [7] of organometallic precursors ($Fe(acac)_3$ [8], Fe-oleate [9], Fe-carboxylate [10], Fe-pivalate [11], or heterodoped ferrite pivalate [12, 13]) in high-boiling solvents at elevated temperatures (~200–360°C). Despite the popularity of the conventional basic

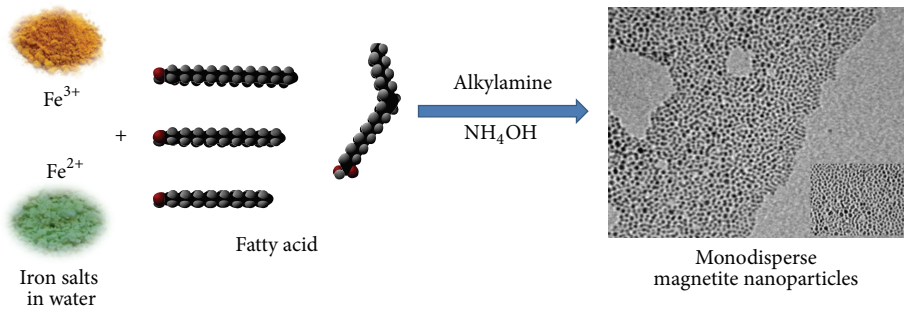

Scheme 1: Synthetic route for the preparation of monodisperse magnetite metal oxide nanoparticles.

coprecipitation method, there remain difficulties in achieving size-controlled, narrowly dispersed, and reproducible nanocrystalline particles [1, 3, 4]. Magnetic nanoparticles tend to aggregate because of strong magnetic dipole-dipole attractions between particles combined with van der Waals forces and high surface energies. The complexity of controlling the nucleation and the unlimited growth of the NPs after nucleation, along with the complicated hydrolysis reactions of iron precursors, makes it difficult to control the size distributions and morphologies of the particles. Some progress on the precipitation of stabilized NPs using capping agents (i.e., small organic molecules [14] and polymers or block copolymers [15]) has been exploited to improve on size distributions, stabilities, and dispersibilities. Nevertheless, majority of the resulting materials formed using the hydrolytic routes were practically agglomerated and uncontrolled [14–17]. To overcome these setbacks, marked improvements in size control, uniformity, and monodispersity have been achieved using organic-based thermolysis procedures. However, the use of expensive polyalcohol components as the iron reducing agent causes many side reactions of polyaldehydes and polyorganic acids, hence making the process of separating the byproducts complicated. Moreover, the use of high-temperature reactions is in practice dangerous and limits the choice of the nanoparticle capping agents. In short, these high-temperature thermolysis methods are complicated, costly, toxic, and industrially limited [17] and usually lead to nanocrystals with relatively low magnetization [18]. Thus, there is some incentive to use simpler, faster, safer, and more practical strategies to efficiently produce M^3NPs.

Inspired by the previous works, we herein describe a convenient route based on basic hydrolytic *in situ coprecipitation* (*Ko-precipitation*) of fatty acid-stabilized ionic metal salts, aided by the presence of alkylamines, to prepare multigram quantities of stabilized M^3NPs colloids dispersed in organic solvents (see Scheme 1). By varying the experimental parameters such as the concentration of fatty acid and the amount of alkylamine added, good control over key physical properties such as particle size (tunable from 2 to 10 nm diameter) and morphology (from agglomerated, monodispersed to elongated) was achieved. The method described here can potentially open new opportunities for the preparation of metal oxide nanoparticles of many different oxide systems, simply by using a wide range of cheap metals salts.

2. Materials and Methods

2.1. Materials. Unless otherwise indicated, all chemicals and solvents were obtained from commercial suppliers and used as supplied without further purification. Iron (III) chloride hexahydrate ($FeCl_3{\cdot}6H_2O$), iron (II) chloride tetrahydrate ($FeCl_2{\cdot}4H_2O$), and the other metal (II) chloride salts ($SrCl_2{\cdot}6H_2O$, $CoCl_2{\cdot}6H_2O$, $NiCl_2{\cdot}6H_2O$, and $ZnCl_2$), oleic acid (OA), hexylamine (HA), and 28% ammonium hydroxide (NH_4OH), were all purchased from either Sigma-Aldrich, LobaChemie, Alfa Aesar, BioBasic Inc., or Techno Pharmchem. Fatty acid chlorides (hexanoyl chloride, caproyl chloride, lauroyl chloride, palmitoyl chloride, and stearoyl chloride) were purchased from Aldrich and subsequently converted to their respective carboxylic acids. Poly-*N*-vinylpyrrolidone (PVP) (average M.W. 58,000) was purchased from Alfa Aesar and tetrabutylammonium tetrafluoroborate ($TBA^+BF_4^-$) from Aldrich. All reactions for the synthesis of M^3NPs were carried under an argon atmosphere. Distilled hexane and double distilled water were used.

2.2. Characterization. X-ray diffraction (XRD) patterns were recorded using Bruker D8 Diffractometer using Cu Kα radiation (λ = 0.154060 nm) and 2θ scan range from 10 to 70°. Fourier transform infrared spectroscopy (FTIR) spectra (400–4000 cm^{-1}) were recorded as KBr pellet forms using Shimadzu IR Affinity-1. Thermal gravimetric analysis (TGA) were carried out on SDT 2960 simultaneous DTA-TGA equipment and the samples were burned in air at a constant heating rate of 10°C/min from 35 to 700°C. Dynamic light scattering (DLS) measurements were assessed on Malvern Zetasizer Nano ZS instrument. Magnetic measurements were recorded on a PPMS AC/DC Magnetometry System (ACMS) manufactured by Quantum Design. The dried samples were exposed to direct current magnetic fields in stepwise increments. The hysteresis curves were obtained at 298 K with an applied field between −20.0 and 20.0 kOe. Transmission electron microscopy (TEM) images were collected on a JEOL-JEM 1230 operating at 100 kV using Gatan camera with Digital Micrograph Imaging software. High-resolution TEM (HR-TEM) were recorded on a JEOL-2100 electron microscope operating at an accelerating voltage of 200 kV. Samples were prepared by depositing 5 μL of the particle dispersion onto 400 mesh Formvar/Carbon-supported copper grid.

The suspension was then allowed to air-dry overnight before images were taken. Optical images were recorded on Nikon inverted optical microscopy supplied with a digital camera.

2.3. Syntheses of Fatty Acid-Stabilized Fe_3O_4 M^3NPs

2.3.1. Large-Scale Synthesis of OA-Stabilized Fe_3O_4 M^3NPs. 250 mL aqueous solution of ferric chloride hexahydrate (50 g, 0.185 mol) and oleic acid (150 g, 0.531 mol, and 3x-fold) were mixed and magnetically stirred under argon for 20 min. Hexylamine (150 g, 1.48 mol) was then added during which the emulsive mixture turns rusty reddish. To the above mixture, aqueous solution of ferrous chloride tetrahydrate (18.4 g, 0.0925 mol) was injected in a molar ratio of Fe(III)/Fe(II) = 2, and the mixture was heated to 80°C. At this point, ammonium hydroxide (30%) was added until pH of ~12 was reached and vigorously stirred overnight. The black precipitate of M^3NPs formed was cooled to room temperature by removing the heat source, isolated *via* centrifugation (4500 rpm, 10 min), washed 3 times with 1-propanol and ethanol, respectively, and redispersed in hexane. Centrifugation (4500 rpm, 20 min) was then applied to remove any undispersed residue. The large-scale stable colloidal hexane solution of Fe_3O_4 M^3NPs was stored at ambient conditions for several months. No precipitation was evident over the course of months. Running the reactions at 25°C or for longer times had no major effects on the dispersity of the small-scale particles. However, we found heating at 80°C for large-scale synthesis was necessary to magnetically stir and solubilize the precursors.

2.3.2. Synthesis of OA1-Stabilized Fe_3O_4 M^3NPs. In a generalized procedure, 5 mL aqueous solution of ferric chloride hexahydrate (0.27 g, 1.0 mmol) and oleic acid (0.424 g, 1.50 mmol) were mixed and magnetically stirred under argon in a degassed vial for 15 min. Hexylamine (0.81 g, 8.0 mmol) was then injected during which the emulsive biphasic mixture turns rusty reddish. After that, the Fe^{2+} precursor and ferrous chloride tetrahydrate (0.10 g, 0.50 mmol) were added and the mixed solution was heated to 80°C. After stirring for a few minutes, ammonium hydroxide (30%) (~3 mL) was added to the mixture until pH of ~12 was reached and vigorously stirred for 90 min. The black precipitate started to form instantly after NH_4OH addition confirming the formation M^3NPs. The black precipitate of M^3NPs formed was cooled to room temperature by removing the heat source, isolated *via* centrifugation (4500 rpm, 10 min), washed 3 times with 1-propanol and ethanol, respectively, and redispersed in hexane. Centrifugation (4500 rpm, 20 min) was then applied to remove any undispersed residue. The stable colloidal hexane solution of ~6 nm Fe_3O_4 M^3NPs was stored at ambient conditions for several months. No precipitation over the course of months was observed.

2.3.3. Synthesis of OA3-, OA5-, and OA10-Stabilized Fe_3O_4 M^3NPs. The same as the procedure described above, however, the concentration of oleic acid was changed to 4.5 mmol (3x-fold), 7.5 mmol (5x-fold), and 15 mmol (10x-fold) to produce 4 nm, 3 nm, and 2 nm sized Fe_3O_4 NPs, respectively.

2.3.4. Synthesis of OA-Stabilized MFe_2O_4 M^3NPs (M = Sr, Co, Ni, and Zn). The same as the procedure for the synthesis of iron oxide NPs, using a constant OA concentration of 7.5 mmol (5x-fold), for example, when Co(II) salt was used instead of Fe(II), ultra-small sized $CoFe_2O_4$ nanocrystals were obtained.

2.3.5. Synthesis of Saturated Fatty Acid-Stabilized Fe_3O_4 NPs. In a generalized procedure, ferric chloride hexahydrate (0.27 g, 1.0 mmol) and ferrous chloride tetrahydrate (0.10 g, 0.50 mmol) dissolved in 5 mL water were mixed with 1.50 mmol of different saturated fatty acids (i.e., stearic acid-C_{18}, palmitic acid-C_{16}, lauric acid-C_{12}, capric acid-C_{10}, and hexanoic acid-C_6) and magnetically stirred under argon in a degassed vial for 15 min. If necessary, minimum amount of DMF is added to solubilize the fatty acid. Ammonium hydroxide (30%) (~3 mL) was slowly added until pH of ~12 was reached and the mixture was heated to 80°C and vigorously stirred for 90 min. The black precipitate of fatty acid-stabilized NPs formed was cooled to room temperature by removing the heat source, isolated *via* centrifugation (4500 rpm, 10 min), washed 3 times with 1-propanol and ethanol, respectively, and redispersed in hexane. Centrifugation (4500 rpm, 20 min) was then applied to remove any undispersed residue. The stable colloidal hexane solution of fatty acid-stabilized Fe_3O_4 NPs was stored at ambient conditions for several months. Precipitation of the particles occurred depending on the length of the fatty acid chain. It was found that at least C_{16} is required to keep the Fe_3O_4 stabilized in hexane for months. For the synthesis in the presence of HA, the same procedure was followed with the addition of 8.0 mmol of HA.

2.4. Synthesis of PVP-Stabilized Hydrophilic Fe_3O_4 M^3NPs.

To render the particles water-soluble, 2 ways were explored: (a) modified double-exchange protocol using $TBA^+BF_4^-$/PVP or (b) direct PVP exchange of the OA capped on the surface of $Fe_3O_4M^3$NPs. In either case, the samples were successfully suspended in water and no precipitation was evident over the course of weeks, with much lower yields and low PVP coating (~17% weight loss as evident from TGA) obtained for route b. (a) *Two-step exchange*: 1 mL of OA-stabilized Fe_3O_4 (10 mg/mL) in hexane was evaporated and redispersed in 1 mL toluene. 4 mL of $TBA^+BF_4^-$ solution (0.09 mM in H_2O : DMF 5 : 1) was then added and the biphasic mixture was gently shaken at room temperate. After 1 hr, the particles were observed to be transferred from the organic to the aqueous layer. The NPs were isolated via pipette, centrifuged, washed repeatedly, and redispersed in 2 mL DMF. 60 mg of PVP with few drops of sodium hydroxide (1 M) was then added to the above 2 mL DMF suspension of $TBA^+BF_4^-$@Fe_3O_4 NPs, and the reaction was stirred for 2 hrs at 37°C. The NPs were centrifuged, washed repeatedly, and redispersed in water to yield colloidal water-soluble PVP-stabilized Fe_3O_4. (b) *Direct exchange*: 1 mL of OA-stabilized

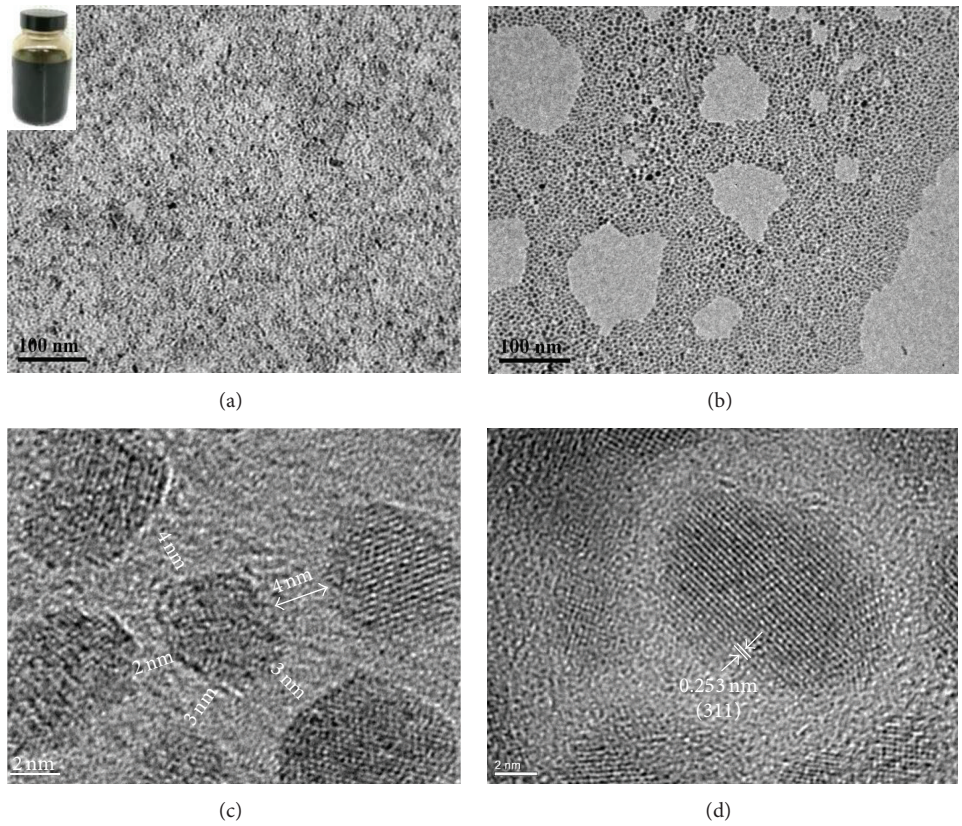

Figure 1: TEM and HR-TEM images of the large-scale production of OA-stabilized M^3NPs of iron oxide at different magnifications. (a) 75 k, (b) 150 k, (c) 800 k, and (d) 1000 k. TEM images revealed the uniformity, and monodispersity of the particles and HR-TEM images showed the highly crystalline nature of the OA-separated NPs showing a single Fe_3O_4 NP with interfringe spacing of 0.253 ± 0.32 nm.

Fe_3O_4 (10 mg/mL) in hexane was evaporated and redispersed in 1 mL toluene. 5 mL of PVP solution (30 mg/mL) containing few drops of sodium hydroxide (1 M) was then added, and the reaction was stirred for 2 hrs at 37°C. The NP dispersion was isolated *via* pipette, centrifuged, washed repeatedly, and then redispersed in water to form stable dispersions with low yields.

3. Results and Discussion

3.1. "Ko-Precipitation Hydrolytic Basic" Method to Prepare OA-Stabilized Fe_3O_4 M^3NPs. The major difficulty for the production of colloidal M^3NPs lies in designing simple, practical, economical, and safe approach to produce large quantities of monodisperse magnetite nanoprobes that are stable for months and do not precipitate from their dispersions. The other key factor is to get those nanocolloids as uniform as possible with good control over size and morphology. Our experimental design reported here is inspired by the well-documented concept of concomitant basic coprecipitation of ferric and ferrous salts in water, combined with the possibility of using alkyl carboxylic acid surfactants as efficient binding stabilizers on the surface of M^3NPs. The so-called "*Ko-precipitation Hydrolytic Basic (KHB)*" method described consists of the following components: inexpensive metallic ions dissolved in aqueous media, long-chain fatty acid surfactants (saturated or unsaturated), cosurfactants (alkylamines), and a base. In a specific reaction, iron oxide NPs were prepared by coinjecting 1 : 0.5 aqueous molar ratios of Fe(III) to Fe(II) salts, different concentrations of oleic acid (OA) (1.5–15 mmol), followed by the addition of hexylamine (HA) (8 mmol) into the mixture, stirred vigorously under inert atmosphere. Addition of excess ammonium hydroxide (NH_4OH) base allowed the formation of ultra-small, ultra-stable, and well-dispersed NPs of iron oxide. The particle size can be tuned from 2 to 10 nm by controlling the OA to iron precursor molar ratios. The obtained nanocrystals are isolated and purified by simple centrifugation without size-selective purifications [19] and are readily dispersed in nonpolar solvents for months. Figure 1(a) shows TEM images of a typical sample of ~4-5 nm sized OA-stabilized iron oxide NPs synthesized at large scale (50 g of ferric salt), indicating the ordered packing and good uniformity achieved (no obvious aggregation was observed over the entire TEM grid). A photograph of the stable colloidal iron oxide hexane dispersion is also shown (inset of Figure 1(a)). When a drop of the nanocrystal dispersion is deposited onto the TEM copper grid at lower concentration, islands made of self-assembled nanocrystals were observed (see Figure 1(b)). Inspection of the products by high-resolution

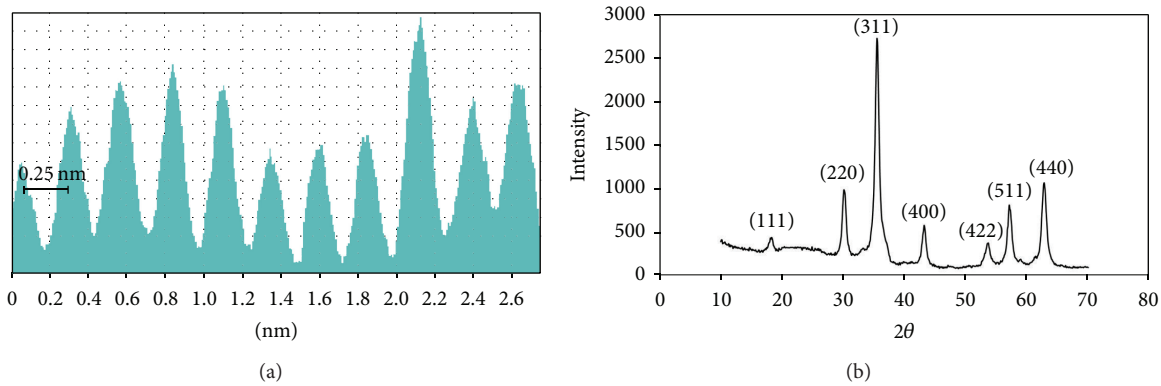

FIGURE 2: (a) Inter-fringe spacing (0.253 ± 0.32 nm) obtained by HR-TEM analysis of a single OA-stabilized nanocrystal of iron oxide at 1000 K. (b) Powder XRD of OA-stabilized M^3NPs of iron oxide. The observed diffraction peaks coincide with the Jade database (JCPDS #019–0629) indicating that the NPs are magnetite (Fe_3O_4).

TEM (HR-TEM) indicates that the NPs show close-packed 2D array of relatively monodisperse sized particles with narrow size distribution (<9%) and a neighbor spacing of ~3.5 nm (±1 nm) maintained by the hydrophobic capping groups (see Figure 1(c)). Further analysis on HR-TEM images clearly shows the lattices of the NPs, indicating that each particle is a well-ordered single crystal despite their small size (see Figure 1(d)). In fact, the distance between two adjacent lattice fringes obtained by HR-TEM analysis of a single nanocrystal is calculated to be 0.253 ± 0.32 nm corresponding to the lattice spacing of (311) planes of magnetite [20] (see Figure 2(a)). XRD of the material revealed that the observed diffraction pattern is in good agreement with published data for Fe_3O_4 magnetite (JCPDS #019–0629), with reflection planes of 111, 220, 311, 400, 422, 511, and 440 clearly identified and 440 peak position centered at 62.5° [21] (see Figure 2(b)). The proof of OA coating on the surface of M^3NPs was confirmed by FTIR (see Figure 3). FTIR spectra showed that OA-stabilized Fe_3O_4 NPs have the distinctive characteristic absorption bands of magnetite (~585 cm^{-1}), with peaks at 1405, 1517, 2850, and 2915 cm^{-1} ascribed to the asymmetric and symmetric C-O stretching vibrations of COO^- and C-H stretching mode of methyl and methylene groups, respectively. The observed shifts indicated that the carboxylate of OA is bound symmetrically to the surface of Fe_3O_4 NPs in a chelating bidentate mode, as has been suggested before [22]. TGA revealed a ~5% weight loss for a weakly bound surfactant layer, followed by ~65% of a tightly held OA layer, further confirming the observed stabilization and solvation of OA-stabilized M^3NPs in organic solvents [23] (inset of Figure 3). In brief, we produced high quality hydrophobically stabilized magnetic metal oxide nanocolloids through a one-pot hydrolytic process by sequentially mixing inexpensive and nontoxic precursors at low temperatures, aging them for a short period of time, and finally collecting them without the use of complicated size sorting processes. According to our knowledge, such TEM images of nearly monodisperse stabilized Fe_3O_4 M^3NPs prepared *via* the coprecipitation of metal salts using hydrolytic synthetic routes have not been reported earlier.

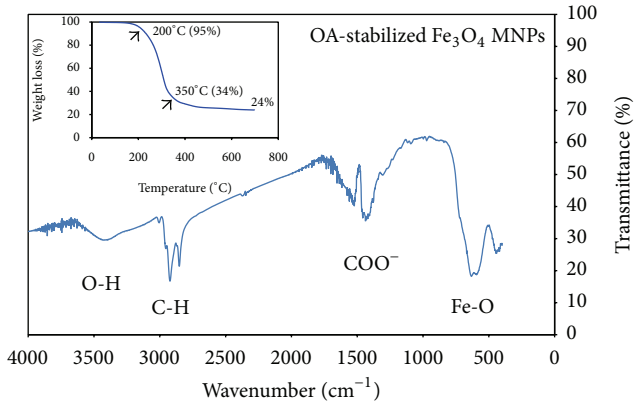

FIGURE 3: FTIR spectra for OA-stabilized Fe_3O_4 M^3NPs. The spectra clearly show the intensity of the characteristic vibrational modes ascribed to OA molecules (inset: TGA analysis of OA-stabilized M^3NPs exhibited a weight loss ~24%, implying the successful coating of the as-synthesized M^3NPs with OA).

3.2. Syntheses and Characterization of the Different Sized OA-Stabilized Fe_3O_4 M^3NPs. The size and monodispersity of the product were found to be strongly dependent on the experimental conditions such as the concentration of OA and the amount of HA added. It was found that when the concentration of OA was increased by factors of 3, 5 and 10, both the size and the morphology of the NPs were affected. For instance, using 1.5 mmol (1x), 4.5 mmol (3x), and 7.5 mmol (5x) of OA during the reaction (with all other parameters fixed), we synthesized M^3NPs with core diameters of ~6 nm, 4 nm, and 3 nm, respectively (see Figure 4). Similar phenomenon was observed earlier, where the nanocrystal size was found to decrease, when the amount of fatty acid (i.e., decanoic acid) was increased [24]. When no OA (0 mmol) was added, the particles were harvested as polydisperse agglomerates of bigger sizes (10–15 nm) dispersed in aqueous media, rather than in organic solvents (see Figure 4(a)). On the other end, once the OA concentration is too high (15 mmol), streak-like packing aggregates of NPs were observed with worm-like

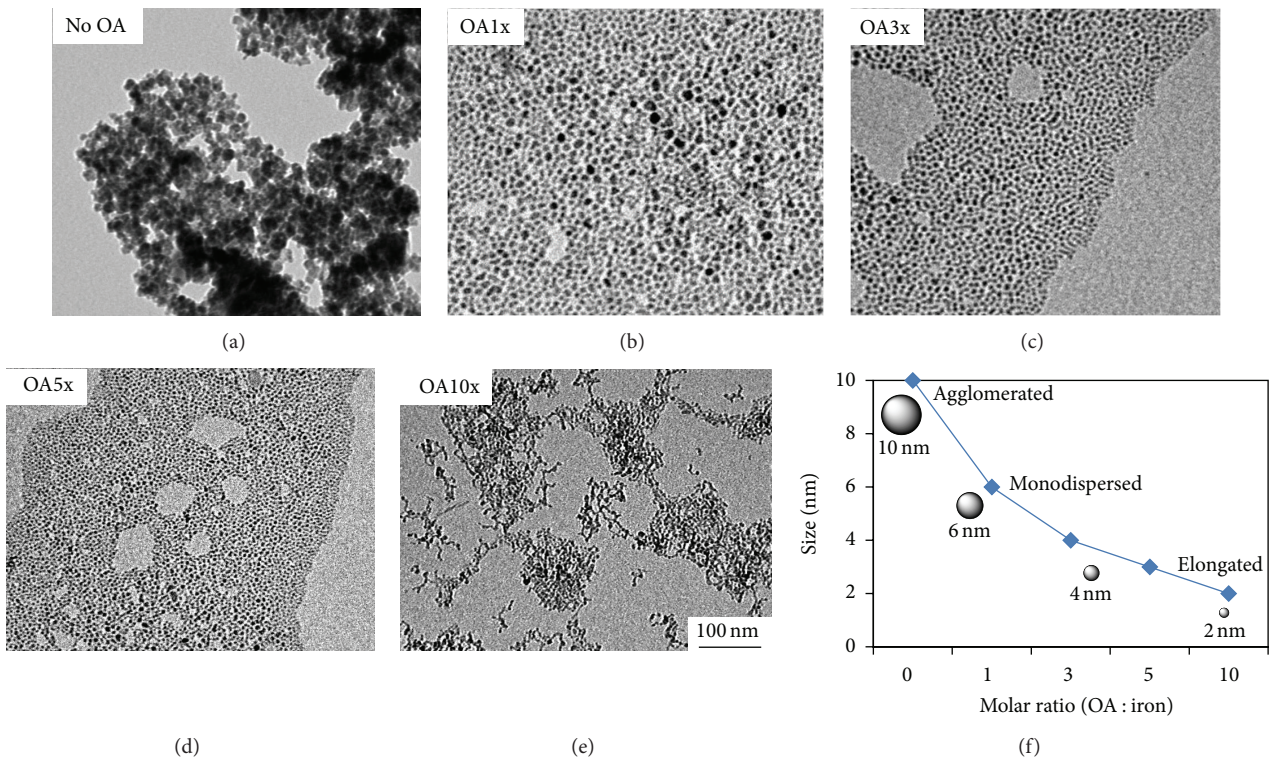

Figure 4: TEM images of the different sized OA-stabilized M^3NPs of iron oxide prepared by varying the ratios of OA to the iron precursor. (a) No OA (0 mmol OA), (b) 1x (1.5 mmol OA), (c) 3x (4.5 mmol OA), (d) 5x (7.5 mmol OA), and (e) 10x (15 mmol OA). (f) Summary of the morphological and size variations of OA-stabilized M^3NPs with increasing OA to iron precursor ratios (0, 1, 3, 5, and 10).

elongated morphologies (see Figure 4(e)). Those nanoparticles resemble the nanoworms obtained from dextran-coated particles prepared *via* the conventional coprecipitation route [25] and are composed of linear aggregates of 2 nm iron oxide cores. Figure 4(f) summarizes the morphology and size variations of the OA-stabilized M^3NPs with increasing OA to iron precursor ratios (0, 1, 3, 5, and 10). DLS measurements of the nanocrystal dispersions in hexane revealed that the size of M^3NPs decreases as the OA concentration increases, further confirming the role due to the hydrophobic density of OA capping during the synthesis. DLS clearly showed sharp peaks at ~5, 10, and 15 nm for the different samples, with no noticeable aggregation (see Figure 5 and Table 1). The ultra-small 2 nm NP streaks, however, were characterized with rather large size distributions and higher polydispersities as depicted from DLS measurements and polydispersities values, probably due to their elongated morphologies formed. Moreover, DLS measurements were recorded for a time period of 12 months showing no significant changes in the size (inset of Figure 5), confirming the remarkable stability of the particles in their organic dispersions for months. In summary, it is best to keep the concentrations of OA at the fivefold limit to obtain nearly monodisperse NPs.

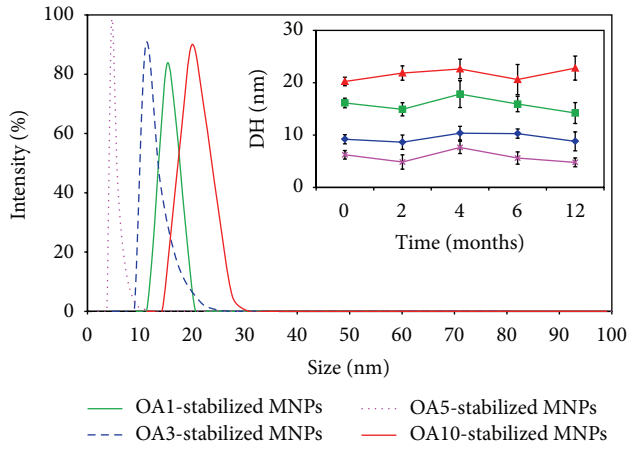

Figure 5: DLS measurements of the different sized OA-stabilized M^3NPs in hexane dispersions. The data clearly shows that as the (OA) molar ratios increase, the particle size decreases. However, once OA10x (i.e., 15 mmol OA) was reached, the size increases to ~20 nm, due to the worm-like streaks of aggregates formed.

Next, magnetization of the different sized Fe_3O_4 M^3NPs with their ultra-small sizes was measured. Field-dependent magnetization curves obtained at 298 K showed a characteristic superparamagnetic behavior with a strong induced magnetizations (M_s = 80 to 43 emu/g_{Fe}) (see Figure 6), higher than the values typically observed for ultra-small iron oxide nanocrystals [26], indicating a high degree of their magnetic ordering and crystallinity and pinpointing

Table 1: Physiochemical properties of the different sized OA-stabilized Fe_3O_4 MNPs.

Sample	Weight loss (%)	Diameter (nm) in hexane	PDI	Morphology
No OA added	N/A	N/A	N/A	Large aggregates
OA1-stabilized MNPs	24%	15.9 ± 1.37	0.202	Monodisperse
OA3-stabilized MNPs	15%	10.4 ± 0.816	0.137	Monodisperse
OA5-stabilized MNPs	19%	5.60 ± 1.17	0.099	Monodisperse
OA10-stabilized MNPs	22%	20.6 ± 2.16	0.377	Elongated aggregates

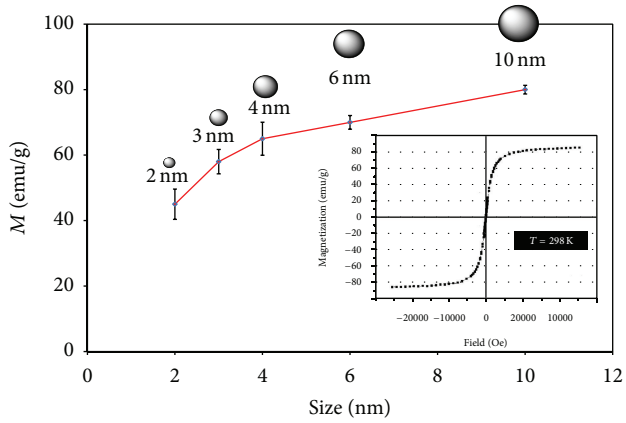

Figure 6: Plot of induced magnetizations for the different sized OA-stabilized M^3NPs (inset: representative field-dependent magnetization (M-H) curve showing the characteristic superparamagnetic behavior). With the reduction of the particle size and the increase in the OA concentration, magnetization decreased from 80 emu/g_{Fe} reaching 43 emu/g_{Fe}, which is higher than the values typically observed for their respective ultra-small iron oxide nanocrystals.

their promise as T1 contrast agents in magnetic imaging. As expected, with the reduction of the particle size and the increase in the OA concentration, magnetization decreased reaching 43 emu/g_{Fe}. It is evident that, in the presence of an external magnetic field (H), these NPs can be easily magnetized to reach their M_s, but when H is removed, their magnetization becomes randomized and the overall moment drops back to zero, making them extremely stable in dispersion states and ready to be used for biomedical applications.

3.3. Effect of Alkylamine on the Synthetic Procedure. Further experiments suggested that the morphology of the product has also a strong dependence on the presence of HA. When the synthesis is conducted without HA, no effective transfer to the organic layer was observed and the product resembles oil-in-water (o/w) micelle system. The particles were harvested as micelles containing NPs of bigger sizes (5–15 nm) (see Figure S1 in the Supplementary Material available online at http://dx.doi.org/10.1155/2015/620672). It was also observed that the yield of the obtained OA-stabilized M^3NPs dissolved in organic solvents increased as the concentration of HA increases (~20% yield when 1.5 mmol HA added *versus* >90% yields for 8 mmol HA). From the above findings, it was concluded that the presence of HA during the synthesis at 8 mmol or above is crucial to afford individual monodisperse nanocrystals. All the above results pinpoint the important roles of both OA and HA to control the size, dispersity, and morphology of the nanocrystals. According to our knowledge, the ability to control the size of Fe_3O_4 M^3NPs using different concentrations of OA in a surfactant-assisted aqueous sol-gel synthesis has not been reported.

3.4. Effect of Fatty Acid Alkyl Chain on the Stability of Fe_3O_4 M^3NPs. To better understand the effect of the alkyl chain on colloidal stability, we prepared a library of NPs coated with saturated fatty acids of different carboxyl alkyl chains RCOOH (R = octadecyl down to hexyl), without the addition of HA. Respective TEM images are shown in Figure 7, showing bigger particles with more marked agglomerations (see Table S1 for DLS measurements of the different fatty acid-stabilized M^3NPs). This observation is in agreement with previously published data, where the size of nanocrystals was found to be bigger when shorter alkyl chains were used [27]. The stability of the particles seems to depend on the alkyl chain, with a minimum of C16 acid needed to effectively stabilize the particles for months (see Figure 7(a)). The long-chain length acids (C16 and C18) appear to be the best suited for particle derivatization with marked stabilization in their hexane dispersions. As a result, we chose stearic acid and studied the effect of HA addition to the synthetic procedure. As expected, we found that the uniformity, polydispersity, and size are clearly affected. TEM images of stearic acid-stabilized $Fe_3O_4M^3$NPs prepared with or without the addition of HA, under identical experimental parameters are shown (see Figure 7(b)).

3.5. Proposed Mechanism of Formation of Fatty Acid-Stabilized Fe_3O_4 M^3NPs. Figure 8 illustrates the formation mechanism of the Fe_3O_4 M^3NPs formed. Upon the addition of the alkylamine HA, a color change into brownish emulsion with a phase transfer of the metal cations into the oily phase is observed. Phase transfer of metal ions from an aqueous to an organic phase using alkylamines has been elegantly demonstrated [28]. Weak adsorption of alkylamine to the iron/iron oxide surface was proposed [29] and recently proven [30], indicating an amine-surface interaction *via* electron donation from the nitrogen lone pair to the positively charged iron ions. With the aid of the HA agent, the ionic metal components become compartmentalized and isolated by the fatty

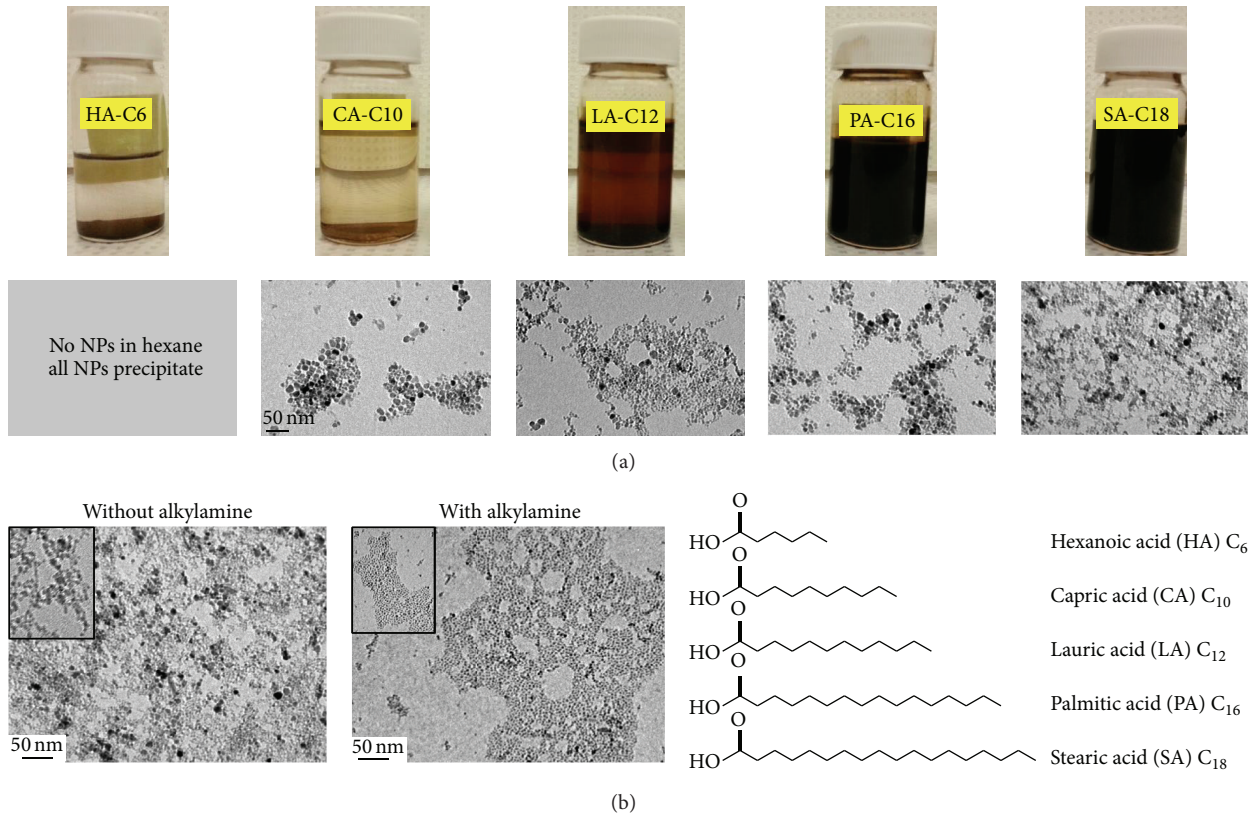

FIGURE 7: (a) TEM images along with photographs of the different fatty acid-stabilized M^3NPs (i.e., stearic acid-C_{18}, palmitic acid-C_{16}, lauric acid-C_{12}, capric acid-C_{10}, and hexanoic acid-C_6) at the same magnification (scale bar = 50 nm). (b) TEM images of stearic acid-stabilized Fe_3O_4 M^3NPs with or without the addition of HA (insets are images with higher magnifications). The images clearly show the effect of HA on the size, uniformity, and dispersity of the synthesized particles.

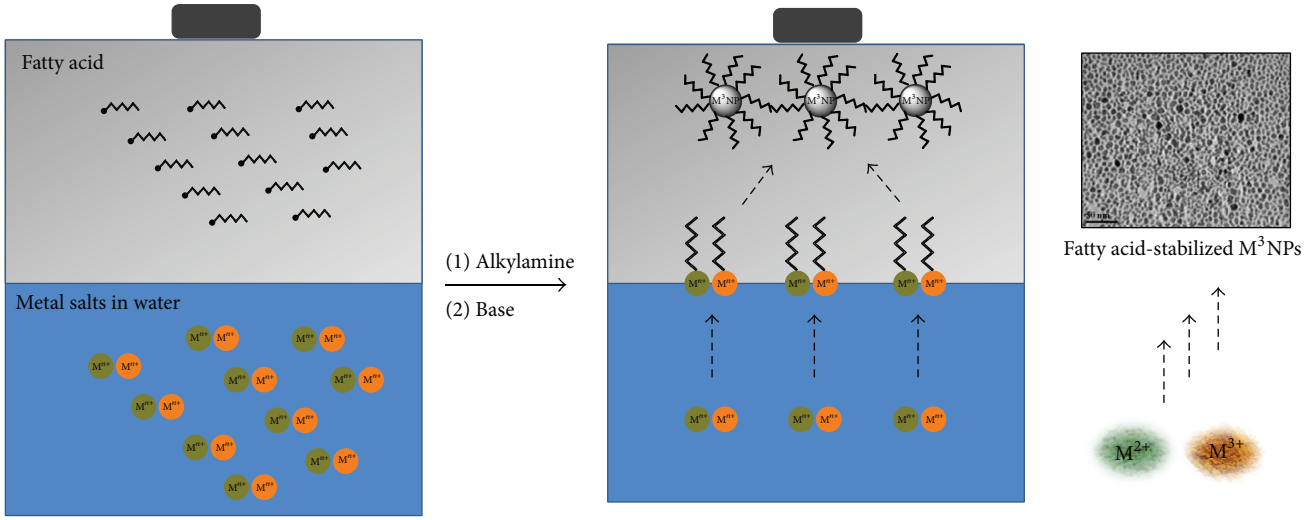

FIGURE 8: Schematic representation of the formation mechanism of the fatty acid-stabilized M^3NPs, aided by the presence of alkylamine as the structure-directing and pulling agent.

acids, acting as steric barriers and protective stabilizers. *Ko*-precipitation by the base generates tiny oxide nuclei at the interfaces, which subsequently form well-ordered dispersions of fatty acid-capped black metal oxide nanocrystals. Since the precursors become spatially separated at the water-oil interface, crystal growth can be limited and agglomerations can be inhibited in favor of small, well-dispersed particles. The formation of thermodynamically stable crystalline colloidal

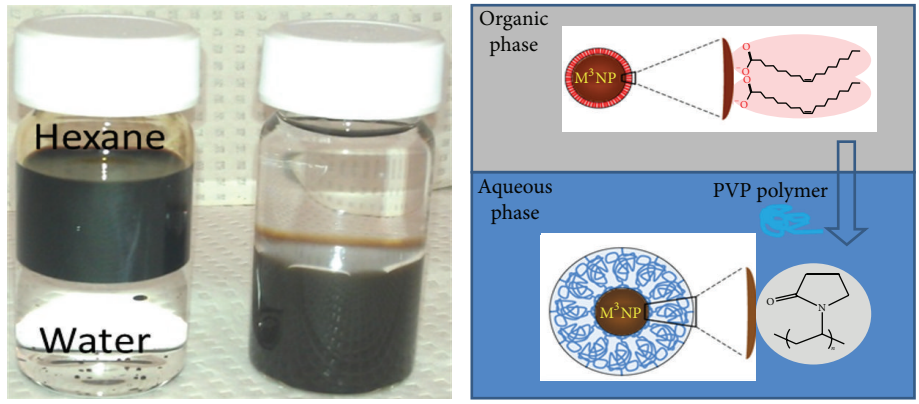

(a)

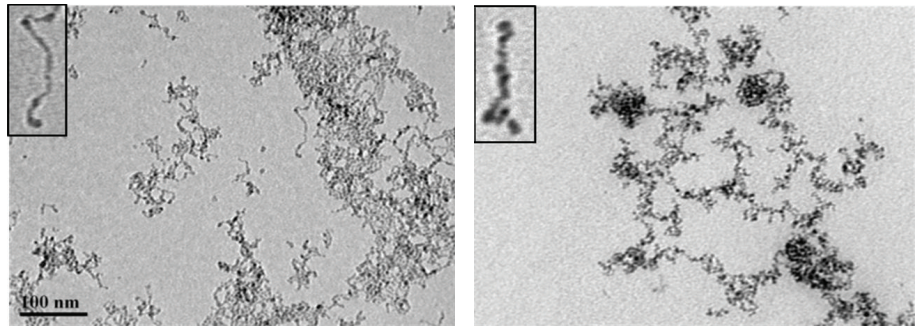

(b)

FIGURE 9: (a) Schematic representation of the transfer from the organic to the aqueous phase along with a photograph showing the successful transfer of OA-stabilized Fe_3O_4 M^3NPs dispersed in hexane to PVP-stabilized Fe_3O_4 M^3NPs dispersed in water. (b) left: TEM image of worm-like OA-stabilized M^3NPs deposited from hexane dispersion; right: TEM image of PVP-stabilized M^3NPs deposited from water dispersion. The insets are magnifications at 250 K.

materials from solution is usually explained by the nucleation and growth theory and has been very recently described for the coprecipitation of magnetite from alkaline one-phase aqueous solutions [31]. In our method, nanocrystals are small-sized and narrowly distributed, possibly due to the hydrolytic reacting environment, the nature of the capping agents, and the relatively low reaction temperatures [32]. In a two-phase system, since the precursors become spatially separated at the water-oil interface, crystal growth can be limited and agglomerations can be inhibited in favor of small, well-dispersed particles. Moreover, the capping agents will disintegrate agglomerates after phase transfer and form stable colloids. In fact, no growth of the particles was observed, even if the reaction was kept for 48 hrs, pinpointing the protective role of the fatty acid coating and blocking crystal growth, as has been suggested earlier. Thus, a nucleation event induced by injecting the base, followed by surfactant-mediated controlled growth, is anticipated [32]. In this way, the agglomerations of NPs that usually occur in typical one-phase aqueous procedures are overcome.

3.6. Generalization of the Method. We have shown that it is possible to prepare dispersible nanocrystals of various metal oxides by our method. We successfully synthesized nanocrystals of doped ferrite metal oxides MFe_2O_4 (M = Sr, Co, Ni, and Zn) resulting in ~2 nm sized nanodots as evident from the TEM images (Figure S2). Experimentally, the same procedure was followed using the corresponding metal (II) chloride salts instead of the Fe(II) precursor. Preliminary results suggest that this simple and cost-effective method described here could be developed into a generalized strategy for the preparation of metal oxide nanoparticles of many different oxide systems. A wide range of cheap metals salts already exists and provides a potential source of readily available precursors for the syntheses of single and complex metal oxides. Apparently, studies and characterization of our samples are currently in progress with the ability to extend this experimental procedure to a wider range of binary transition metal oxides.

3.7. Preparation of Hydrophilic Fe_3O_4 M^3NPs for Biomedical Applications. For biomedical endpoints, we attempted extraction of the NPs from their organic dispersions into their aqueous phase using a ligand-exchange process [33]. Owing to its biocompatibility, biodegradability, and protective properties, poly-*N*-vinyl-pyrrolidone-grafted iron oxide NPs have been shown to be very useful for cellular uptake, imaging, and delivery [34]. Herein, we replaced the OA-stabilized Fe_3O_4 M^3NPs with PVP (Figure 9(a)), based on a modified procedure of a recently reported work [35], using the weak

tetrabutylammonium tetrafluoroborate ($TBA^+BF_4^-$) binder as the primary phase-transfer agent. A two-step phase transfer was accomplished by shaking a biphasic mixture of OA-stabilized M^3NPs in TBA^+BF_4, followed by PVP treatment in aqueous solution. Direct PVP exchange in the absence of $TBA^+BF_4^-$ resulted in very little exchange, justifying the necessity of $TBA^+BF_4^-$ treatment, in parallel with earlier observations [35]. Figure 9(b) shows TEM image of the PVP-stabilized Fe_3O_4 M^3NPs before and after OA exchange, showing negligible change to the NP features, indicating the stability during the ligand-exchange process. DLS for the PVPylated Fe_3O_4 M^3NPs as water suspension depicted a hydrodynamic radius $D_H = 56 \pm 5.05$ nm (see Figures S3). FTIR and TGA further confirmed the stripping of the OA coating and its exchange with the PVP polymer (see Figures S4 and S5). FTIR spectra showed that the intensity of the characteristic vibrational modes ascribed to OA molecules dramatically decreased after PVPylation, with a shift in the vibrational band from 1517 to 1660 cm^{-1} belonging to C=O group of PVP. Moreover, TGA showed a ~50% weight loss of the PVP-coated M^3NPs, with an initial weight loss up to 385°C due to the desorption of the residual physically adsorbed OA layer. The weight loss from 385 to 700°C is due to PVP polymers and their subsequent degradation releasing CO_2 gas. Thus, it is believed that the iron oxide complex *via* either coordination bond formation through its carbonyl group or weak covalent interaction with PVP, as has been suggested before [36].

4. Conclusions

In summary, we embarked on a simple, practical, scalable, and economical synthetic methodology to prepare different sized fatty acid-stabilized M^3NPs of ferrites in water phase without the routine of using high-boiling point solvents and elevated temperatures. Nontoxic and inexpensive reactants such as metal salts were employed. No heating up to 200–300°C was performed. M^3NPs were produced with noticeable stability, high magnetizations, narrow size distributions, and tailor-made versatility. Different sizes and morphologies of M^3NPs were prepared by varying the experimental parameters, mainly the fatty acid and alkylamine. Moreover, the presence of alkylamine additive was found to be a key in order to produce ultra-small and monodisperse M^3NPs. Preliminary results showed that our procedure could offer the possibility of a generalized approach to the production of doped ferrite nanocrystals. Upon coating with water-soluble polymers, the small-sized particles become biologically relevant, with great promise for theranostic applications as imaging and magnetically targeted drug delivery vehicles.

Conflict of Interests

The authors declare no conflict of interests regarding the publication of this paper.

Acknowledgments

The authors acknowledge financial support by KSAU-HA and KAIMRC through Grant RC13/204/R. Special thanks are due to Dr. Abdulmohsen Al-Kushi (KSAU-HS), Dr. Barrak Somaie (KAIMRC), and Dr. Ahmed Al-Askar (KAIMRC) for the continuous support. They thank Maram Al-Haidar and the premed undergraduates Abdulaziz Al-Otaibi, Abdulrahman Al-Kabli, and Rayan Al-Onazi for their help in the synthesis of M^3NPs. They are grateful to Chair Dr. Tarek Ghaddar (AUB) and Leane Hachem (Université de Poitiers) for their assistance in conducting TGA and magnetization measurements. Last but not least, many thanks are to National Guard Hospital for the generous timeslots on the TEM.

References

[1] A.-H. Lu, E. L. Salabas, and F. Schüth, "Magnetic nanoparticles: Synthesis, protection, functionalization, and application," *Angewandte Chemie—International Edition*, vol. 46, no. 8, pp. 1222–1244, 2007.

[2] Y.-W. Jun, J.-H. Lee, and J. Cheon, "Chemical design of nanoparticle probes for high-performance magnetic resonance imaging," *Angewandte Chemie—International Edition*, vol. 47, no. 28, pp. 5122–5135, 2008.

[3] M. H. El-Dakdouki, K. El-Boubbou, J. Xia, H. Kavunja, and X. Huang, "Methods for magnetic nanoparticle synthesis and functionalization," in *Chemistry of Bioconjugates*, pp. 281–314, John Wiley & Sons, 2014.

[4] B. L. Cushing, V. L. Kolesnichenko, and C. J. O'Connor, "Recent advances in the liquid-phase syntheses of inorganic nanoparticles," *Chemical Reviews*, vol. 104, no. 9, pp. 3893–3946, 2004.

[5] R. Massart, "Preparation of aqueous magnetic liquids in alkaline and acidic media," *IEEE Transactions on Magnetics*, vol. 17, no. 2, pp. 1247–1248, 1981.

[6] M. H. El-Dakdouki, K. El-Boubbou, M. Kamat et al., "CD44 targeting magnetic glyconanoparticles for atherosclerotic plaque imaging," *Pharmaceutical Research*, vol. 31, no. 6, pp. 1426–1437, 2014.

[7] S. Sun, C. B. Murray, D. Weller, L. Folks, and A. Moser, "Monodisperse FePt nanoparticles and ferromagnetic FePt nanocrystal superlattices," *Science*, vol. 287, no. 5460, pp. 1989–1992, 2000.

[8] S. Sun and H. Zeng, "Size-controlled synthesis of magnetite nanoparticles," *Journal of the American Chemical Society*, vol. 124, no. 28, pp. 8204–8205, 2002.

[9] J. Park, K. An, Y. Hwang et al., "Ultra-large-scale syntheses of monodisperse nanocrystals," *Nature Materials*, vol. 3, no. 12, pp. 891–895, 2004.

[10] N. R. Jana, Y. Chen, and X. Peng, "Size- and shape-controlled magnetic (Cr, Mn, Fe, Co, Ni) oxide nanocrystals via a simple and general approach," *Chemistry of Materials*, vol. 16, no. 20, pp. 3931–3935, 2004.

[11] K. Abdulwahab, M. A. Malik, P. O'Brien et al., "Synthesis of monodispersed magnetite nanoparticles from iron pivalate clusters," *Dalton Transactions*, vol. 42, no. 1, pp. 196–206, 2013.

[12] K. O. Abdulwahab, M. A. Malik, P. O'Brien et al., "Hot injection thermolysis of heterometallic pivalate clusters for the synthesis

of monodisperse zinc and nickel ferrite nanoparticles," *Journal of Materials Chemistry C*, vol. 2, no. 33, pp. 6781–6789, 2014.

[13] K. O. Abdulwahab, M. A. Malik, P. O'Brien et al., "A one-pot synthesis of monodispersed iron cobalt oxide and iron manganese oxide nanoparticles from bimetallic pivalate clusters," *Chemistry of Materials*, vol. 26, no. 2, pp. 999–1013, 2014.

[14] M. Mahdavi, M. B. Ahmad, M. J. Haron et al., "Synthesis, surface modification and characterisation of biocompatible magnetic iron oxide nanoparticles for biomedical applications," *Molecules*, vol. 18, no. 7, pp. 7533–7548, 2013.

[15] J. S. Basuki, A. Jacquemin, L. Esser, Y. Li, C. Boyer, and T. P. Davis, "A block copolymer-stabilized co-precipitation approach to magnetic iron oxide nanoparticles for potential use as MRI contrast agents," *Polymer Chemistry*, vol. 5, no. 7, pp. 2611–2620, 2014.

[16] X. Gu, Y. Zhang, H. Sun, X. Song, C. Fu, and P. Dong, "Mussel-inspired polydopamine coated iron oxide nanoparticles for biomedical application," *Journal of Nanomaterials*, vol. 2015, Article ID 154592, 12 pages, 2015.

[17] Y. Lee, J. Lee, C. J. Bae et al., "Large-scale synthesis of uniform and crystalline magnetite nanoparticles using reverse micelles as nanoreactors under reflux conditions," *Advanced Functional Materials*, vol. 15, pp. 503–509, 2005.

[18] J. Ge, Y. Hu, M. Biasini, W. P. Beyermann, and Y. Yin, "Superparamagnetic magnetite colloidal nanocrystal clusters," *Angewandte Chemie International Edition*, vol. 46, no. 23, pp. 4342–4345, 2007.

[19] B. Kowalczyk, I. Lagzi, and B. A. Grzybowski, "Nanoseparations: strategies for size and/or shape-selective purification of nanoparticles," *Current Opinion in Colloid and Interface Science*, vol. 16, no. 2, pp. 135–148, 2011.

[20] L. Zeng, W. Ren, J. Zheng, P. Cui, and A. Wu, "Ultrasmall water-soluble metal-iron oxide nanoparticles as T_1-weighted contrast agents for magnetic resonance imaging," *Physical Chemistry Chemical Physics*, vol. 14, no. 8, pp. 2631–2636, 2012.

[21] J. Jing, Y. Zhang, J. Liang et al., "One-step reverse precipitation synthesis of water-dispersible superparamagnetic magnetite nanoparticles," *Journal of Nanoparticle Research*, vol. 14, no. 4, article 827, 2012.

[22] S. Xuan, L. Hao, W. Jiang, X. Gong, Y. Hu, and Z. Chen, "Preparation of water-soluble magnetite nanocrystals through hydrothermal approach," *Journal of Magnetism and Magnetic Materials*, vol. 308, no. 2, pp. 210–213, 2007.

[23] R. Tadmor, R. E. Rosensweig, J. Frey, and J. Klein, "Resolving the puzzle of ferrofluid dispersants," *Langmuir*, vol. 16, no. 24, pp. 9117–9120, 2000.

[24] J. Zhang, S. Ohara, M. Umetsu, T. Naka, Y. Hatakeyama, and T. Adschiri, "Colloidal ceria nanocrystals: a tailor-made crystal morphology in supercritical water," *Advanced Materials*, vol. 19, no. 2, pp. 203–206, 2007.

[25] J.-H. Park, G. von Maltzahn, L. Zhang et al., "Magnetic iron oxide nanoworms for tumor targeting and imaging," *Advanced Materials*, vol. 20, no. 9, pp. 1630–1635, 2008.

[26] B. H. Kim, N. Lee, H. Kim et al., "Large-scale synthesis of uniform and extremely small-sized iron oxide nanoparticles for high-resolution T1 magnetic resonance imaging contrast agents," *Journal of the American Chemical Society*, vol. 133, no. 32, pp. 12624–12631, 2011.

[27] Y.-W. Jun, Y.-M. Huh, J.-S. Choi et al., "Nanoscale size effect of magnetic nanocrystals and their utilisation for cancer diagnosis *via* magnetic resonance imaging," *Journal of the American Chemical Society*, vol. 127, no. 16, pp. 5732–5733, 2005.

[28] J. Yang, E. H. Sargent, S. O. Kelley, and J. Y. Ying, "A general phase-transfer protocol for metal ions and its application in nanocrystal synthesis," *Nature Materials*, vol. 9, pp. 683–689, 2009.

[29] J. Cheon, N.-J. Kang, S.-M. Lee, J.-H. Lee, J.-H. Yoon, and S. J. Oh, "Shape evolution of single-crystalline iron oxide nanocrystals," *Journal of the American Chemical Society*, vol. 126, no. 7, pp. 1950–1951, 2004.

[30] M. H. Wood, R. J. L. Welbourn, T. Charlton, A. Zarbakhsh, M. T. Casford, and S. M. Clarke, "Hexadecylamine adsorption at the iron oxide-oil interface," *Langmuir*, vol. 29, no. 45, pp. 13735–13742, 2013.

[31] J. Baumgartner, A. Dey, P. H. H. Bomans et al., "Nucleation and growth of magnetite from solution," *Nature Materials*, vol. 12, no. 4, pp. 310–314, 2013.

[32] N. T. K. Thanh, N. Maclean, and S. Mahiddine, "Mechanisms of nucleation and growth of nanoparticles in solution," *Chemical Reviews*, vol. 114, no. 15, pp. 7610–7630, 2014.

[33] J. Yang, J. Y. Lee, and J. Y. Ying, "Phase transfer and its applications in nanotechnology," *Chemical Society Reviews*, vol. 40, no. 3, pp. 1672–1696, 2011.

[34] J. Huang, L. Bu, J. Xie et al., "Effects of nanoparticle size on cellular uptake and liver MRI with polyvinylpyrrolidone-coated iron oxide nanoparticles," *ACS Nano*, vol. 4, no. 12, pp. 7151–7160, 2010.

[35] A. Dong, X. Ye, J. Chen et al., "A generalized ligand-exchange strategy enabling sequential surface functionalization of colloidal nanocrystals," *Journal of the American Chemical Society*, vol. 133, no. 4, pp. 998–1006, 2011.

[36] X. Lu, M. Niu, R. Qiao, and M. Gao, "Superdispersible PVP-coated Fe_3O_4 nanocrystals prepared by a "one-pot" reaction," *Journal of Physical Chemistry B*, vol. 112, no. 46, pp. 14390–14394, 2008.